Moisture absorption characteristics of a SiO_2 film from 2 to 3 μm

Yun Cui (崔 云)*, Hao Li (李 豪), Kui Yi (易 葵), and Jianda Shao (邵建达)

Key Laboratory of Materials for High Power Laser, Shanghai Institute of Optics and Fine Mechanics, Chinese Academy of Sciences, Shanghai 201800, China

**Corresponding author: cuiyun@siom.ac.cn*

Received July 31, 2014; accepted November 28, 2014; posted online February 9, 2015

We prepare SiO_2 coatings on different substrates by either electron-beam evaporation or dual ion-beam sputtering. The relative transmittances of the SiO_2 coatings are measured during the heating process. The SiO_2 coating microstructures are studied. Results indicate that the intensity and peak position of moisture absorption are closely related to the microstructures of the coatings. The formation of microstructures depends not only on the preparation process of the coatings but also on the substrate characteristics.

OCIS codes: 310.4925, 310.6860, 140.3070.
doi: 10.3788/COL201513.023101.

Infrared lasers operating within the 2–3 μm wavelength range have various applications, such as in medical equipment[1,2], space remote sensing[3–5], optical communication[6], and gas detection. Growing demands in the fields of offensive and defensive space applications as well as strong field laser physics have led to the development of broadband, tunable, ultra-short, and ultra-intense mid-infrared lasers. A large coefficient of water absorption is a noteworthy property of this band. Relevant to this research field is the fact that different forms and hydrates of water considerably influence the optical properties, internal stress[7], and laser irradiation resistance of coatings[8]. However, published research conducted on their adsorption characteristics is uncommon. Adsorption characteristics can help us to deeply understand the mechanism pertaining to how moisture adsorption affects film performance. In this Letter, we report SiO_2 film deposition by two kinds of process on different substrates. The adsorption characteristics and microstructures of the SiO_2 films were detected and analyzed.

An infrared quartz material was selected and deposited on different substrates by electron-beam evaporation (EBE) and dual ion-beam sputtering (IBS). The substrates included fused silica, silicon crystal, and alumina crystal. The parameters of the coating processes are listed in Table 1.

Table 1. Parameters of the Coating Process

Deposition Method	Coating Material	Substrate	Baking Temperature (°C)	Base Pressure (Pa)	O_2 Pressure (Pa)	Thickness (μm)
EBE	SiO_2	Fused quartz, silicon crystal, and alumina crystal	300	5×10^{-3}	1×10^{-2}	2
IBS			70	1×10^{-4}	4×10^{-2}	2

Table 2. Water Vibrations in the Mid-Infrared Spectral Region

Sample	Wavenumber (cm^{-1})	Wavelength (μm)	Vibration Mode	References
Water	3280	3.05	Stretching OH Symmetric, $\nu 1$	[9]
	3490	2.86	Stretching OH Asymmetric, $\nu 3$	
Solid phase of water	3200	3.13	OH stretching of ice structure	[10]
Liquid phase of water	3400	2.94	OH stretching of liquid H_2O structure	
Mesoporous silica	3400	2.94	OH in free H_2O	[11]
	3672	2.72	OH in Si-OH	
Mesoporous silicon oxide	3230	3.10	OH stretching of ice-like structure	[12]
	3400	2.94	OH stretching of liquid H_2O structure	

Spectra as a function of temperature were obtained with a Fourier-transform infrared (FTIR) spectrometer (Nicolet 6700, Thermo Fisher). The FTIR spectrometer had a diffuse reflectance and a high-temperature reaction chamber to observe the desorption process in real time. Scanning was repeated 32 times and the resolution was 4 cm^{-1}. The rate of heating was 10°C/min and the precision of the temperature control was 1°C.

The surface morphologies and coating roughness were determined by atomic force microscopy (AFM; Dimension 3100, Bruker Nano), which had a measurement error within 0.01 nm. Each test site on the samples was scanned over an area of 5 μm × 5 μm. The cross sectional morphologies were observed by focused ion-beam (FIB) field-emission scanning electron microscopy (FESEM; Auiga, Zeiss). The resolution was 1.7 nm when the acceleration voltage was 1 kV.

The respective vibrations we observed from free liquid water, solid water, and adsorbed water are listed in Table 2 in order to compare the vibrations of these three types of water.

Spectral evolution of the coatings during desorption was indicative of different intensities and peak positions of the moisture absorption, as shown in Figs. 1 and 2.

The relative transmittance of the SiO_2 coatings deposited by IBS slightly increased in intensity as the temperature increased. The increasing bands were between 3280 and 3490 cm^{-1} (3.05 and 2.86 μm, respectively). This indicates a vibration mode of OH stretching pertinent to free H_2O (Table 2).

The relative transmittance of the SiO_2 coatings deposited by EBE strongly increased in intensity as the temperature increased. The increasing bands were between 3240

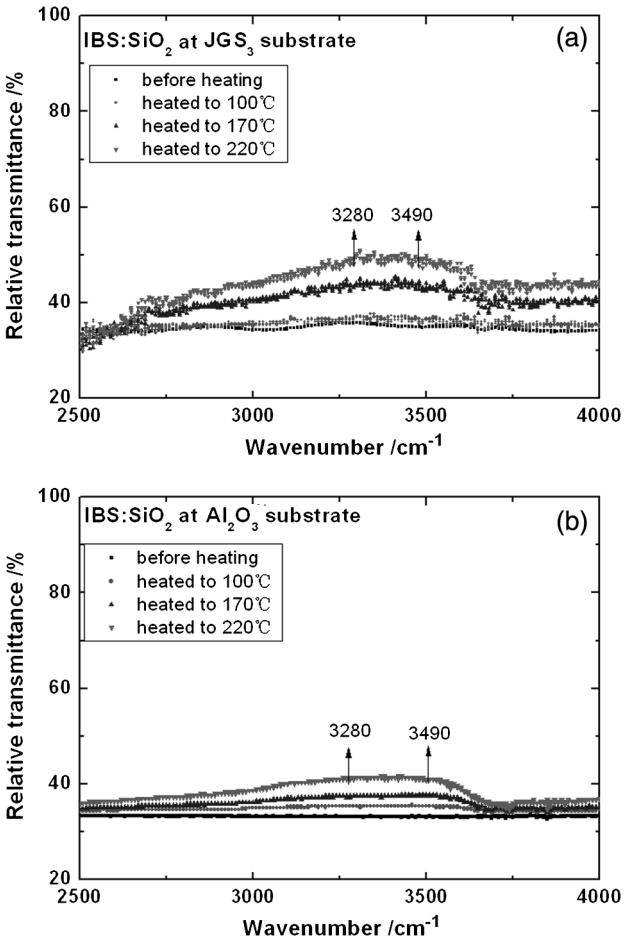

Fig. 1. Variations in the FTIR spectra of SiO_2 coatings deposited by IBS as a function of heating temperature.

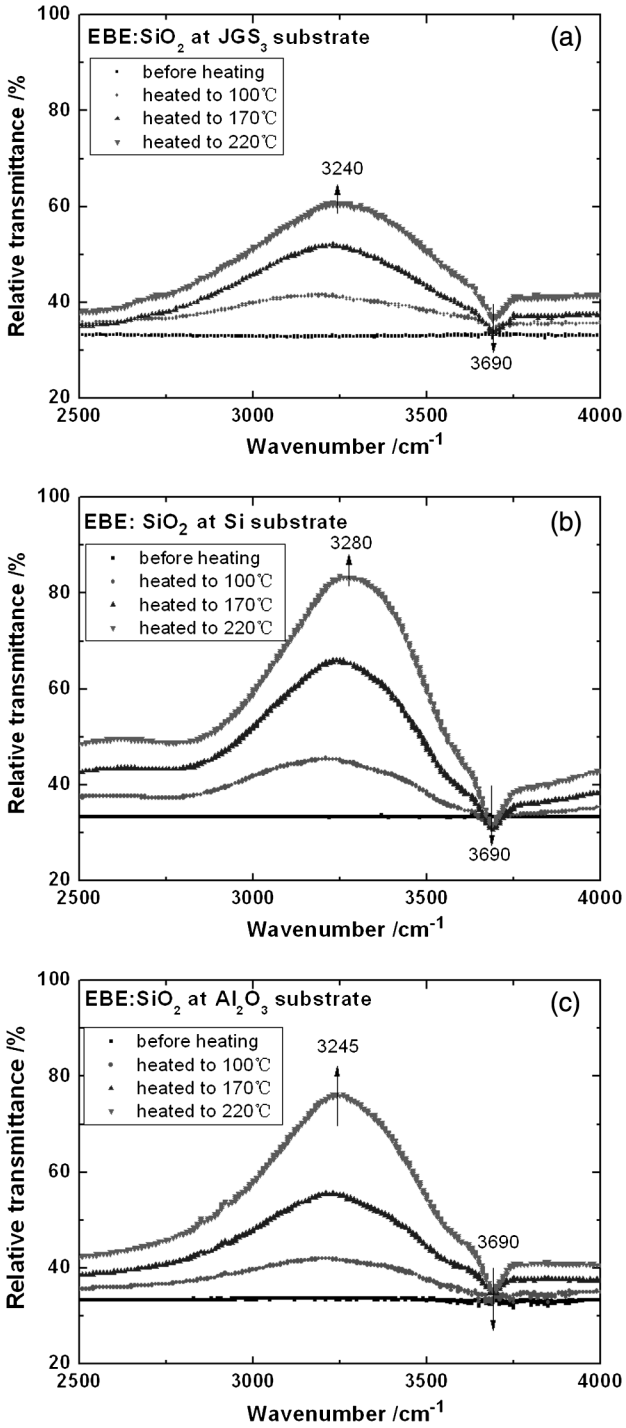

Fig. 2. Variations in the FTIR spectra of SiO_2 coatings deposited by EBE as a function of heating temperature.

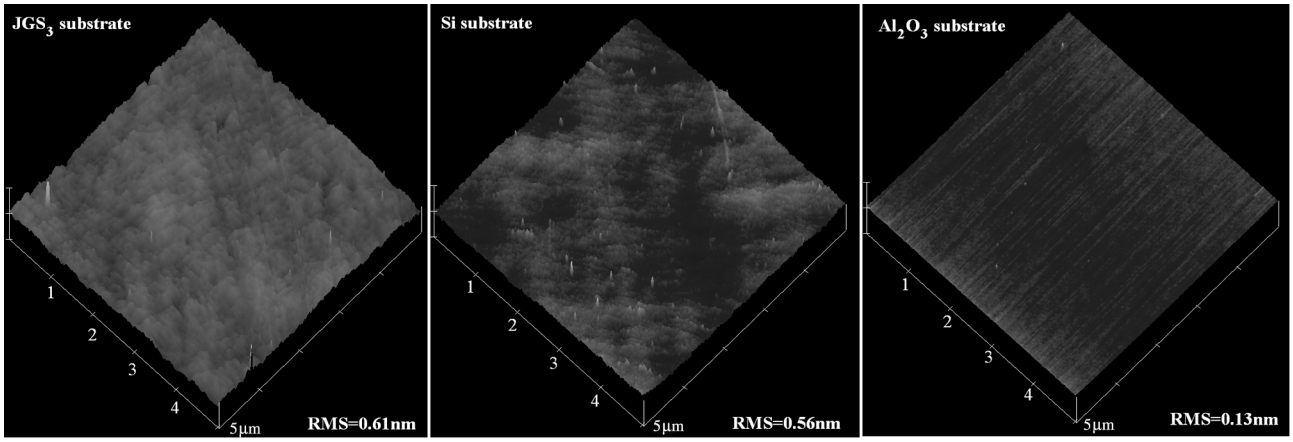

Fig. 3. Surface structures of the different substrates.

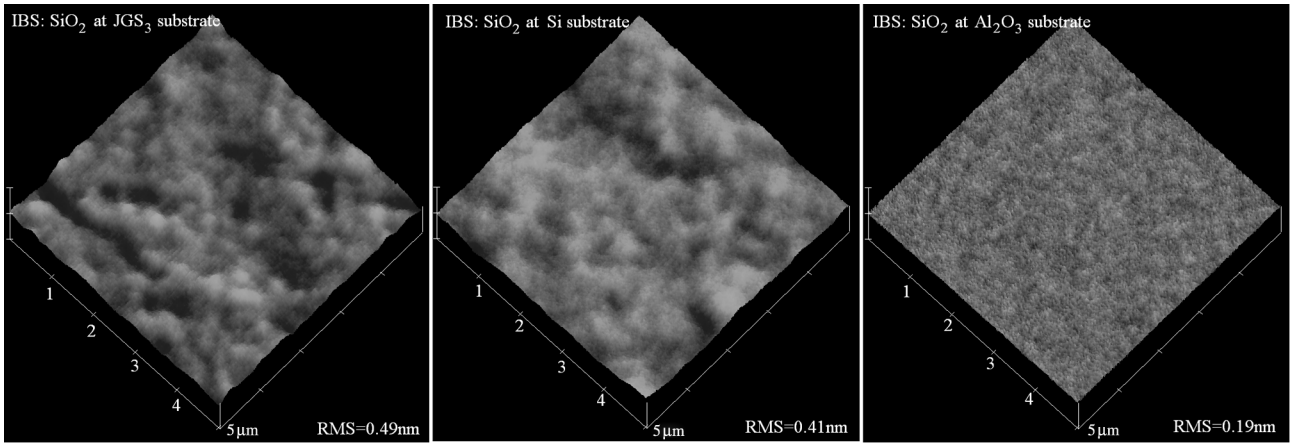

Fig. 4. Surface structures of coatings deposited by IBS on different substrates.

and 3280 cm^{-1} (3.09 and 3.05 μm, respectively). This position corresponds to OH stretching of an ice-like structure (in accordance with the peak position in Table 2). The decreasing bands, at 3690 cm^{-1} (2.71 μm), are attributable to heating-induced Si–OH production.

In order to determine why the relative transmittance changed, the surfaces and cross sectional morphologies of the samples were measured.

As shown in Fig. 3, the root-mean square (RMS) roughness of the substrates was small (no more than 0.61 nm). The surfaces of the fused quartz and silicon crystal were uneven, which imparted a larger RMS than that of the alumina crystal.

Figure 4 shows surface structures of SiO_2 coatings deposited by IBS, and Fig. 5 shows the cross sectional morphology. The RMS roughness was small (no more than 0.49 nm). The coatings on the fused quartz and silicon crystal were uneven because the substrates were uneven. The coating was obviously dense (Fig. 5). Due to the dense structure, moisture could not enter the interior of the coatings and remained on the surface. The change of the relative transmittance was related to a close association between the water and the surface. Consequently, the relative transmittance of the coatings only slightly increased in intensity when we increased the temperature.

Figure 6 shows surface structures of SiO_2 coatings deposited by EBE and Fig. 7 shows the cross-sectional morphology. The RMS roughness was more than 1 nm

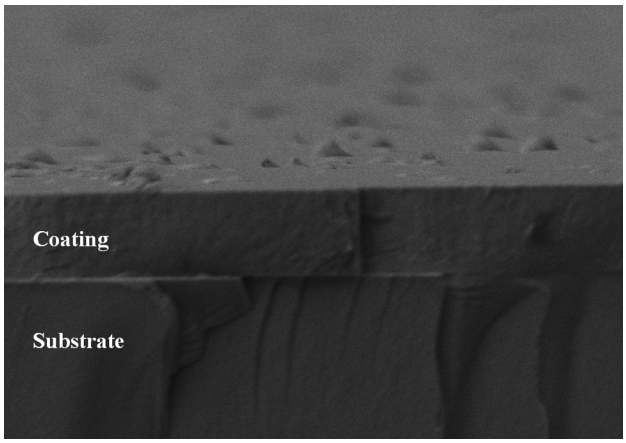

Fig. 5. Scanning electron microscopy (SEM) cross sectional morphology of a coating fabricated by IBS.

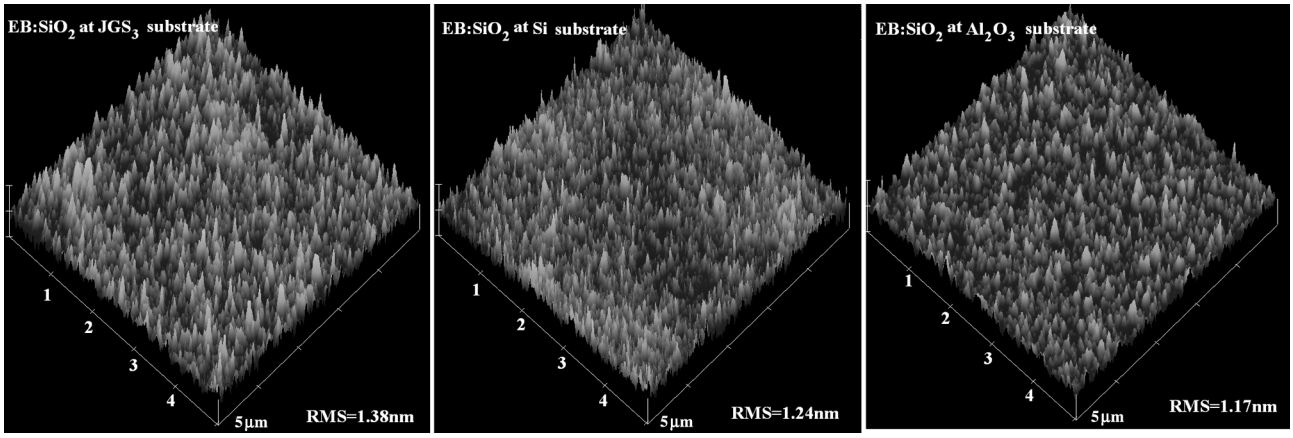

Fig. 6. Surface structures of SiO_2 coatings deposited by EBE on different substrates.

(Fig. 6). The microstructure was columnar and porous (Fig. 7) The RMS roughness was far more than that of the corresponding substrate due to the EBE-induced columnar structure[13]. Due to the columnar and porous structure, absorbed moisture entered the coatings and filled the pores along the columnar structure. Consequently, the relative transmittance of the coatings strongly increased in intensity in accordance with increasing temperature.

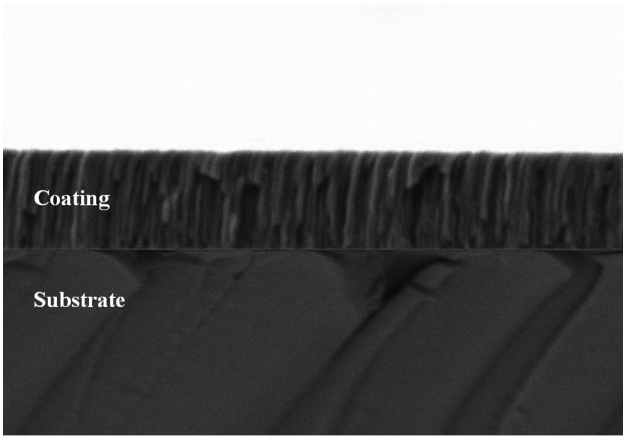

Fig. 7. SEM cross sectional morphology of a coating fabricated by EBE.

The pore sizes of the coatings were analyzed through the "grain size" functional module in our AFM software. The threshold height was set as 2.50 nm. The mean pore sizes of the coatings were between 25 and 30 nm (Fig. 8). When the pore diameters were small (3–20 nm), the structure of H_2O in the mesoporous silicon oxide was affected by both near- and far-surface structures[11]. Therefore, the effects of the interfaces overlapped and were strengthened, causing the water molecules to become more ice-like. The overlap of the interface effect induced formation of a solid-water-solid system. When the pore diameters were large (30–50 nm), the structure of the water was only affected by the near-side surface. Hence, larger pores affected the H_2O molecular structure less than smaller pores.

As indicated in Fig. 8, the pore size of the coatings on the alumina crystal was less than that on the fused quartz and silicon crystal. Preliminary analysis suggested that this was attributable to the different coefficients of thermal expansion between the substrates (Table 3). During deposition, in which the baking temperature was increased

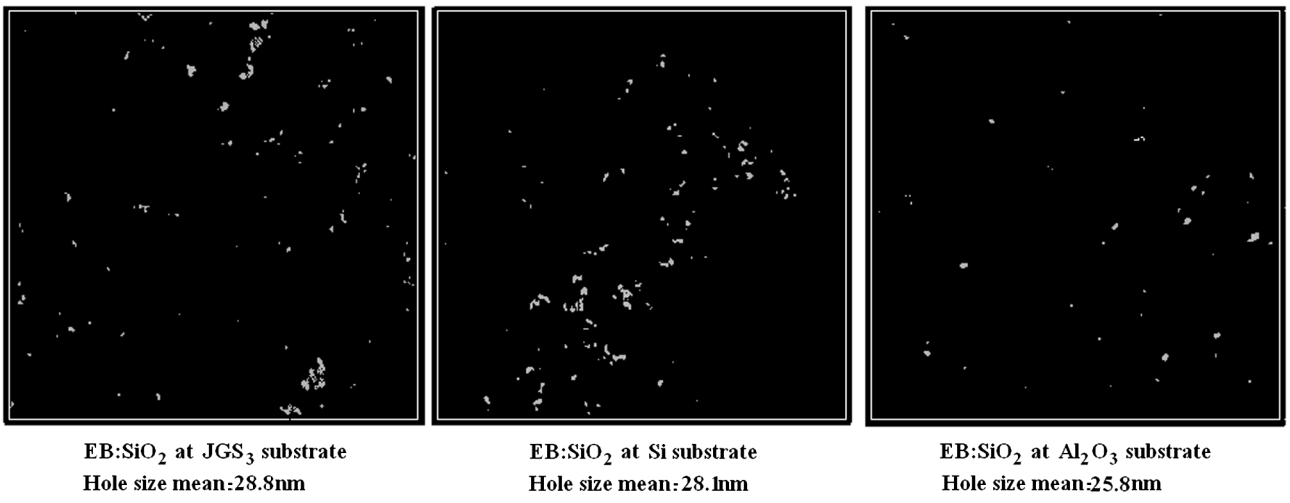

Fig. 8. Mean pore sizes of the SiO_2 coatings prepared by EBE on different substrates.

Table 3. Coefficients of Thermal Expansion of the Substrates and Coating

Material	Coefficient of Thermal Expansion (10^{-6} K)	References
Fused quartz	0.5	[17]
Silicon crystal	3.6	[18]
Alumina crystal	7.3–8.1	[18]
SiO_2 coating prepared by EBE	0.4	[19]

up to 300°C, the coefficient of thermal expansion of the alumina crystal was larger than that of the other substrates. Thus, the contraction of the alumina crystal was more drastic during the cooling process, which led to a smaller pore size. Furthermore, the sharp contraction of the alumina crystal also led to a large amount of stress; thus, cracking and peeling of the SiO_2 coating on the alumina crystal could occur[14–16].

In conclusion, we measure the FTIR spectra of SiO_2 coatings to investigate the forms and hydrates of H_2O in coatings through the heating process. Results show that moisture absorption is largely on the surface of dense coatings fabricated by IBS. Adsorption capacity is obviously low; the absorption peak is similar to that of free H_2O. For coatings that have a columnar and porous structure as induced by EBE, moisture enters the interior of the coatings and fills the pores along the columnar structure. Some Si–OH form due to the interaction between the water molecules and SiO_2. Most of the water molecules become more ice-like due to the coating pore sizes. The mean sizes of the pores in the columnar structure are somewhat variable because of the thermal expansion coefficient of the substrates.

This work was supported by the National Natural Science Foundation of China under Grant No. 61405225.

References

1. M. Natali Cizmeciyan and H. Cankaya, Opt. Lett. **34**, 3056 (2009).
2. Q. Wang, Opt. Lett. **34**, 3616 (2009).
3. P. A. Budni, L. A. Pomeranz, M. L. Lemons, C. A. Miller, J. R. Mosto, and E. P. Chicklis, J. Opt. Soc. Am. B. **17**, 723 (2000).
4. P. A. Budni, M. L. Lemons, J. R. Mosto, and E. P. Chicklis, IEEE J. Quantum Electron. **6**, 629 (2000).
5. G. Renz and W. Bohn, Proc. SPIE **6552**, 655202 (2007).
6. J. Ren, R. Zhou, and S. Lou, Chin. Opt. Lett. **12**, 090605 (2014).
7. E. H. Hirsch, J. Phys. D **13**, 2081 (1980).
8. L. Na, W. Yingjian, and Z. Ming, Chin. Phys. Lett. **27**, 150 (2010).
9. T. Richard, L. Mercury, and F. Poulet, J. Colloid Interface Sci. **304**, 125 (2006).
10. G. E. Ewing, J. Phys. Chem. B **108**, 15953 (2004).
11. J. Abe, N. Hirano, and N. Tsuchiya, J. Mater. Sci. **47**, 7971 (2012).
12. D. B. Asay and S. H. Kim, J. Phys. Chem. B **109**, 16760 (2005).
13. J.-C. Zhang, L.-M. Xiong, F. Ming, and H.-B. He, Chin. Phys. B **22**, 253 (2013).
14. T. Tan, J. Huang, M. Zhan, G. Tian, J. Shao, and Z. Fan, Proc. SPIE **5774**, 555 (2004).
15. T.-Y. Tan, D.-W. Zhang, M.-Q. Zhan, J.-D. Shao, and Z.-X. Fan, Chin. Phys. Lett. **22**, 227 (2005).
16. Z. Deng, H. Gao, L. Xiao, H. He, Z. Fan, and J. Shao, Chin. Opt. Lett. **5**, 60 (2007).
17. H. Tada, A. E. Kumpel, and R. E. Lathrop, J. Appl. Phys. **87**, 4189 (2000).
18. W. M. Vim and R. J. Paff, J. Appl. Phys. **45**, 1456 (1974).
19. C.-C. Lee, C.-L. Tien, and W.-S. Sheu, Rev. Sci. Instrum. **72**, 2128 (2001).